Construction and Building Materials 215 (2019) 544–556

Contents lists available at ScienceDirect

Construction and Building Materials

journal homepage: www.elsevier.com/locate/conbuildmat

# Influence of the nano $TiO_2$ dispersion procedure on fresh and hardened rendering mortar properties

Sérgio Roberto Andrade Dantas [a,b,*], Ramoel Serafini [a], Roberto Cesar de Oliveira Romano [a], Fúlvio Vittorino [b], Kai Loh [a]

[a] Polytechnic School of the University of São Paulo, Department of Civil Construction Engineering, Avenue Prof. Almeida Prado, trav. 2, n° 83, 05424-970, São Paulo, Brazil
[b] Institute of Technological Research, Avenue Prof. Almeida Prado, n° 532, 05508-901, São Paulo, Brazil

## HIGHLIGHTS

- Mortars produced with different $TiO_2$ samples and dispersion conditions.
- Effect of $TiO_2$ in the fresh and hardened state properties of rendering mortars.
- Dispersion condition of $TiO_2$ changes the properties of rendering mortars.
- The properties, in the hardened state, are in function of the dispersion methods and the characteristics of $TiO_2$.
- $TiO_2$ on drying shrinkage control is potentially increased by dispersion.
- The dispersion procedure and characteristics of $TiO_2$ influence on the drying shrinkage.

## GRAPHICAL ABSTRACT

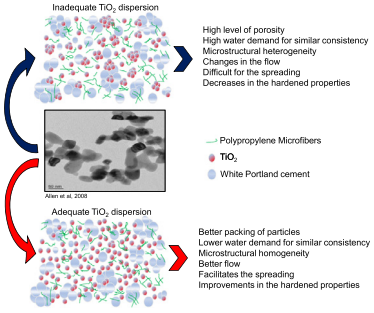


## ARTICLE INFO

*Article history:*
Received 20 August 2018
Received in revised form 20 March 2019
Accepted 24 April 2019
Available online 3 May 2019

*Keywords:*
$n\text{-}TiO_2$
Dispersion condition
Drying shrinkage of mortars
Rendering mortars for the facade
Degradation process

## ABSTRACT

This study was carried out to evaluate the influence of $n\text{-}TiO_2$ dispersion on fresh and hardened rendering mortar properties. Five compositions were evaluated with dispersed polypropylene microfibers (PPMF): a reference, without $n\text{-}TiO_2$ addition, and four using two commercial samples of $n\text{-}TiO_2$, evaluated in two dispersion conditions. Although the materials were the same in all formulations, the water content was modified to maintain the same mortar consistency as determined by flow table results. The fresh properties of the mortars were determined by means of squeeze flow and air-entrainment tests, while hardened properties were evaluated by capillary water absorption, air-permeability, dynamic elastic modulus, drying shrinkage, split tensile strength according to the Brazilian test, and porosity by the Archimedes immersion method. The results obtained have shown that the fresh and hardened mortar properties were affected by the dispersion procedure and the properties of the $n\text{-}TiO_2$ samples, indicating that the addition of $n\text{-}TiO_2$ in a dispersed form was more effective to control fresh and hardened mortar properties. On the other hand, drying shrinkage results are not influenced by the dispersion procedure but as of the characteristics of $n\text{-}TiO_2$.



## 1. Introduction

The uniformity of nanoparticle dispersion into rendering mortar (random or agglomerated) affects the properties of materials.

* Corresponding author at: Department of Civil Construction Engineering, Polytechnic School of the University of São Paulo, Avenue Prof. Almeida Prado, trav. 2, n° 83, 05424-970 São Paulo, Brazil.
*E-mail address:* sergiodantas@usp.br (S.R.A. Dantas).

https://doi.org/10.1016/j.conbuildmat.2019.04.190
0950-0618/

Particle size and shape as well as the method of adding to the mixture, are points of great importance which should be considered.

The rheological properties of dispersions are governed by the microstructure of the system. In those systems, the solid particles are relatively small and the interparticle forces are significantly pronounced to influence the microstructure, the state of aggregation of the dispersion and, consequently, the mechanical and rheological properties of the system [1].

A great impact on the fresh state properties of compositions is generated when n-$TiO_2$ are added in cement-based materials due to the strong tendency towards agglomerate formation due to their ultrafine size [2,3], increasing the water content to mixture and affecting the hardened state properties. Therefore, the addition of n-$TiO_2$ as a dry powder into the cement paste presents difficulties regarding homogeneity due to the dry insertion of the compound. Besides, the n-$TiO_2$ material is wasted since a considerable amount of the product is not available on the surface for photocatalytic activity.

Fine particles, such as n-$TiO_2$, tend to agglomerate due to their low mass and high surface area, factors that cause surface forces to predominate over gravitational forces. According to the DLVO (Derjaguin-Landau-Verwey-Overbeek) theory, the dispersion state of a system of electrically charged particles in a suspension is governed by the sum of the potential energies of attraction and repulsion of the particles [4]. These potential energies are determined by three main characteristics, in order of importance: a) surface electrical charges; b) pH of the medium and c) surface area [5]. As the balance of electric charges on the surfaces of different particles is not always in equilibrium, generated attraction forces are stronger than the those of repulsion [6].

In a road surface pavement application study, the n-$TiO_2$ dispersion accounted for different concrete performances. Nanoparticle addition to the cement matrix caused the formation of agglomerates of low mechanical resistance, while adding the material in a dispersed and "loose" procedure promoted the homogenization of n-$TiO_2$ in concretes [7].

The increase in n-$TiO_2$ particle concentration in the dispersions produces a more viscous suspension, and the increased viscosity could be attributed to the agglomeration of n-$TiO_2$ [8]. In this sense, the use of the concept of particle packing as a strategy for the development of coating mortars can be a great ally as it enables the production of mortars with low cement consumption [9].

The packing models assume that the larger grains form voids that are progressively filled by smaller grains, resulting in high density by reducing the volume of voids between the grains. In addition to particle size distribution and specific surface area, other properties influence particle packing, such as morphology, coarse particle porosity, and particle agglomeration. Therefore, a good granulometric design must be polymodal, where mixing and compaction techniques also influence the porosity of a mixture for a given particle size distribution [6].

Porosity, specific surface area, and solid content are particle properties that influence the fresh and hardened state parameters, as spread, air-incorporation, mechanical strength, modulus of elasticity, permeability, adhesion and others. These are factors that greatly influence mortar capacity of withstanding aggressive agents such as water, oxygen, carbon dioxide, chlorides and aggressive solutions [7]. In this context, not only these parameters can be associated with the service life and durability of a building, but also to evaluate the susceptibility of these fluids to permeate into a porous medium.

The particle dispersion stands as a challenge that needs to be addressed for the addition of nanomaterials in cement matrixes [10]. Regarding the literature data, it becomes obvious that additional factors influence the photocatalytic efficiency of the different n-$TiO_2$ samples. Particle characteristics like size, morphology or surface constitution account for the different photocatalytic activity. In particular, catalyst particle size seems to have noticeable influence on the photocatalytic activity [11].

Thus, the main goal of this study was to experimentally evaluate the influence of n-$TiO_2$ dispersion on fresh and hardened rendering mortar properties.

## 2. Experimental program

### 2.1. Materials

The mortars used in this study were prepared using white Portland cement (WHITE CEM I 52.5R EN 197-1), dolomites #20, #40 and #80, commercial air-entraining agent (AEA) based on sodium lauryl sulphate molecules, water retaining agents based on cellulosic ether molecules, and polypropylene microfibers. The amount of all these raw materials was kept constant, but the water content of each mixture was modified to maintain mortar consistency.

Two different samples of commercial n-$TiO_2$ powder were used in the mixtures, and the comparisons were made using five sets of specimens as described in Table 1.

Ref. represents the composition formulated without the addition of n-$TiO_2$, and the specimens to which P25 and PC105 had been added were marked with a "p" and a "d", which stood for Standard Energy Mix (SEM) and High Energy of Dispersion (HED) respectively.

### 2.2. Methods

#### 2.2.1. Raw material characteristics

The specific surface area (SSA) of materials was measured using the BET method. The equipment used was an $N_2$ gas/vapor adsorption in a Belsorp Max equipment with a pre-treatment of the specimens at a temperature of 60 °C and a pressure of $7 \times 10^{-5}$ MPa for 24 h in a Belprep II – vac equipment. The real density analysis was determined by means of the Helium pycnometry method in a Quantachrome MVP 5DC multipycnometer. Particle size distribution of the finer particles was determined by laser granulometry in a Malvern Mastersizer LongBed with a detection range of 0.1–355 μm, and the dolomites particle size distribution was determined by means of a Dynamic Image Analyser (QicPic – Sympatec) with a detection range of 1–4000 μm. The raw material characteristics are presented in Table 2 and Fig. 1.

Fig. 2 shows the mineralogical composition of white Portland cement and n-$TiO_2$ obtained by X-ray diffraction: IPT 15742 – CT-OBRAS-LMCC-Q-PE-092 – "Mineralogical analysis by X-ray diffraction" and IPT 15458 – Q-PE-089 – "Determination of phases analysis of Portland cement and Portland cement clinker using the Rietveld method of analysis by powder diffraction", according to ASTM guidelines [12]. Equipment used: Rigaku model Windmax 1000, operating on copper Kα rad radiation with 40 kV – 20 mA and 2°/min sweep[1]. Table 3 shows the determined chemical composition according to ABNT and ASTM standards [13–20].

#### 2.2.2. Compositions

The compositions were developed without granulometric changes of coarse particles, but the mobility parameters were affected due to the characteristics of the n-$TiO_2$ used. It should

[1] The compound identification was performed using a Panalytical X-pert HighScore Plus software (version 4.5 (4.5.0.22741), and diffraction patterns and structures provided by the free Crystallography Open Database (COD) database in 2016) and, eventually, diffraction patterns and ICDD (International Center for Diffraction Data) and ICSD (International Center for Structure Data) structures, respectively.

**Table 1**
Specimen description. SEM – mortar mixed using standard energy mix; HED – mortar mixed using high energy of dispersion.

| Mixtures | Description[1] | Specimens | Quant |
|---|---|---|---|
| Ref. | Mortar without n-$TiO_2$ addition (SEM) | cylindrical/prismatic | 05/03 |
| Ref+P25d | Mortar with HED n-$TiO_2$ addition | cylindrical/prismatic | 05/03 |
| Ref+P25p | Mortar with SEM n-$TiO_2$ addition | cylindrical/prismatic | 05/03 |
| Ref+PC105d | Mortar with HED n-$TiO_2$ addition | cylindrical/prismatic | 05/03 |
| Ref+PC105p | Mortar with SEM n-$TiO_2$ addition | cylindrical/prismatic | 05/03 |

[1] All compositions were mixed using dispersed PPMF addition.

be stressed that each composition was mixed with a different amount of water, aiming to maintain the same workability defined in the flow-table tests. The consumption, in kg/m$^3$, of each raw material in the compositions is described in Table 4.

Fig. 3 shows the particle size distribution of each composition, and Table 5 shows the packing and mobility parameters resulted in the proportioning of raw materials. Interparticle separation (IPS) represents the mean distance to separate the finer particles assuming that all are completely dispersed, and maximum paste thickness (MPT) indicates the distance between the coarse particles, having been calculated in this work disregarding the air-voids, but considering the differences in the water content used in each mixing.

The IPS concept is particularly applicable to fine particle suspensions, as in the case of n-$TiO_2$, where surface forces are predominant, considering the effect of particle size distribution and predicting particle contact (d = 0) when the amount of the liquid phase is lower than the porosity of the packaged system [9]. The lower the porosity of the system, regulated by particle size distribution, the higher is the IPS value of the paste and greater is the amount of the free liquid phase to separate the particles [21]. Particle separation must be at least 50 nm for movement to occur [4]. Studies suggest similar values for the water layer between the particles of 41 nm [22] and 45 nm [23] respectively.

To increase the flowability of a mortar, it is necessary to maximize the MPT value to provide the lowest contact among the coarse grains. The MPT has an close relationship with the fresh and the hardened state's properties of coating mortars. For values lower than 20 μm, the compressive loads to spread mortars increases significantly, because the friction between the aggregates is higher. Above this value, the compressive load falls smoothly as a function of the MPT increase, and this value may change according to the specific properties of each mortar evaluated [24,25].

The mobility and packaging parameters were used to define the composition of the mortar, but no correlation was observed with the properties obtained. That fact shows that the characteristics of the products obtained also depend on chemical and surface parameters, which were not considered in this work.

### 2.2.3. Mixing process

Fig. 4 shows the stages used to mix the mortars. The set of mixtures, show only small differences. The mixing procedure of the raw materials used to prepare the specimens is detailed below.

- Reference mortars (mixtures without the addition of n-$TiO_2$): water was added into the bowl of the Hobart N50 mixer, and then microfibers were added and Standard Energy Mix (SEM) applied for the 90 s using: 30 s in speed 1 (low), 30 s in speed 2 (high) and 30 s speed 1 (low). The dry powder was added for 1 min with the equipment turned off. A period of the 30 s was allowed for particle wetting, and then, the equipment was turned on, and the mixing was performed for 90 s using the same procedure described previously.
- Ref+P25p and Ref+PC105p mortars: the n-$TiO_2$ was homogenized with all the dry powder (cement and dolomites) in a plastic bag for the 30 s before the addition. The procedure used to disperse microfibers, add the dry powder and mix the mortar was the same as the reference mortars.
- Ref+P25d and Ref+PC105d mortars: all the water and n-$TiO_2$ were to the added to a metallic vessel, adapted from a cocktail mixer. The suspension was dispersed under High Energy Dispersion (HED) (10.000 rpm with cawles type propellant) for 30 s and, then the microfibers were inserted. From that moment on, the mixing procedure was the same descried previously.

### 2.2.4. Fresh state properties

After mixing, the fresh state properties were evaluated using the flow table test [26], as shown in Fig. 5, squeeze flow test [27] Fig. 6, and air-incorporation by gravimetric method [28].

Squeeze Flow: tests were conducted on a universal testing machine (Instron 5569) with a 1kN load cell. Samples were prepared on a metallic plate with smooth surfaces to ensure a non-absorption condition, and a cylindric mold (diameter of 101 mm and width of 20 mm) was used. The tests were performed using a displacement rate of 0.1 mm/s, to a maximum displacement of 18 mm or maximum load of 1 kN.

Air-entrainment: tests were done according to the gravimetric method, using a 400 ml volume cup and the mass used to fill it was quantified. The values of air entrainment were calculated based on the mortar's water content and the real density of the dry powder.

### 2.2.5. Hardened state properties evaluation

The moulded specimens were cured for 28-days under controlled temperature and humidity (respectively, at 23 °C and 50%). The hardened properties were measured by water absorption by capillarity [29], air-permeability, dynamic elasticity modulus (E) [30], split tensile strength by the Brazilian test method [31],

**Table 2**
Raw material characteristics.

| Materials | Characteristics diameter (μm) | | | Specific surface area | Average density |
|---|---|---|---|---|---|
| | $d_{10}$ | $d_{50}$ | $d_{90}$ | (m$^2$/g) | (cm$^3$) |
| White Portland cement | 2.6 | 17.7 | 19.5 | 0.86 | 3.05 |
| Dolomite #20 | 975.1 | 1242.1 | 1620.5 | 0.16 | 2.90 |
| Dolomite #40 | 24.3 | 230.0 | 739.6 | 0.56 | 2.94 |
| Dolomite #80 | 4.5 | 38.3 | 133.9 | 0.80 | 2.81 |
| n-$TiO_2$ (PC105) | 0.66 | 1.50 | 4.59 | 79.8 | 3.62 |
| n-$TiO_2$ (P25) | 1.38 | 3.90 | 17.67 | 49.4 | 3.84 |

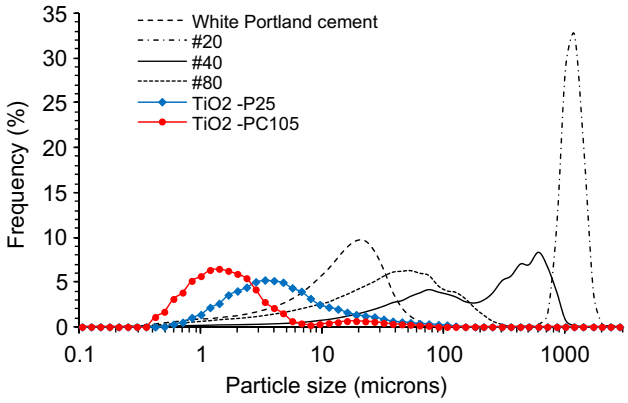


**Fig. 1.** Particle size distributions of materials.

porosity (the Archimedes method) and drying shrinkage test [32]. The results were statistically evaluated using a One-way ANOVA and followed by a Tukey test.

Porosity of specimens: measured according to the Archimedes water immersion test, based on the dry, wet and immersed masses. The mass is determined on the dried specimens after immersion in water and under vacuum for 2.5 h (Fig. 7). The total porosity was calculated according to the Eq. (1), where $\rho_{REL}$ is the relative mortar density obtained by gas He pycnometry.

$$\text{Total porosity}\,(\%) = (1 - -\rho_{REL}) \times 100\% \quad (1)$$

Air-permeability: measured according to the vacuum-decay method [33–36]. The apparatus employed was a vacuum pump connected to a suction chamber that is was in contact with the surface of the mortar. When the vacuum pump is turned on, a transducer registered the pressure variations as a function of time until the pressure stabilized. Specimens were sealed using PVC plastic (Fig. 8a) to guarantee the unidirectional flow. The test starts when the vacuum is turned off, and the time it takes for the applied vacuum pressure to extinguish is quantified (Fig. 8b and c). The permeability (expressed in $k_1$ ($m^2$) values) is was calculated using the Forchheimer equation (Eq. (2)), with respect to two basic hypotheses: negligible air-compressibility and the use of just the linear part of the equation.

$$\frac{\Delta P}{L} = \frac{\mu}{k_1} v_s + \frac{\rho}{k_2} v_s^2 \quad (2)$$

L is the sample thickness, μ and ρ are, respectively, the fluid viscosity and density, vs is the speed of air-percolation and ΔP is the pressure variation, through which vs, μ and ρ are measured or calculated. The term $\rho vs/k_1$ shows the viscous effect of the fluid-solid interaction, while the term $\rho vs^2/k_2$ represents the inertial effects. The terms $k_1$ and $k_2$ are thus known as Darcian and no-Darcian permeability constants, about Darcy's law, a simpler and earlier empirical model for permeability description. However, $k_2$ was not used to compare the results in this work [37].

Dynamic elasticity modulus (E): measured according to the Brazilian standard using a PUNDIT (Portable Ultrasonic Non-destructive Digital Indicating Tester) equipment with 200 kHz frequency transducers and a circular cross-section with a 20 mm diameter.

Split tensile strength: measured according to the Brazilian standard using an Emic DL10000 equipment with a continuously applied load at a rate of 400 N/s until the test specimens rupture, as shown in Fig. 9.

Water absorption by capillarity: the specimen was partially sealed with beeswax at one of their ends at a height of ± 3 cm, to avoid water absorption, thus forcing the water to penetrate only

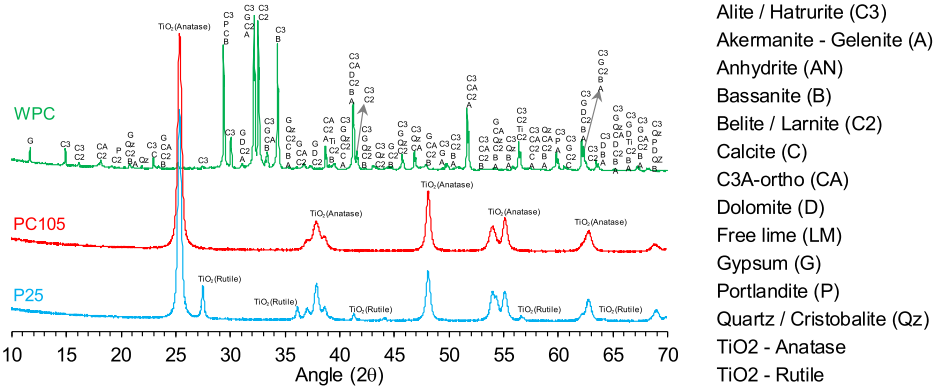


| Phase | ICSD code | ICDD code |
|---|---|---|
| Alite | 81100 / 22501 | - |
| Akermanite – Gelenite | 160345 | - |
| Anhydrite | 27474 | - |
| Bassanite | - | 96-101-0919 |
| Belite | 421708 | - |
| Calcite | - | 96-901-6707 |
| C3A-ortho | 6287 | - |
| Free lime | - | 96-900-6738 |
| Gypsum | 27876 | - |
| Portlandite | 202223 | - |
| Quartz | - | 96-900-6688 |
| $TiO_2$ - Anatase | 93098 / 202243 | - |
| $TiO_2$ – Rutile | 51938 | - |

**Fig. 2.** X-ray diffraction of white Portland cement and $TiO_2$.

**Table 3**
Chemical composition of cement and n-$TiO_2$ samples.

| Compound | White CEM I (%) | Limited NBR-12989/93 | P25 | PC105 |
|---|---|---|---|---|
| LOI | 2.48 | ≤27.0 | – | – |
| $TiO_2$ | – | – | 99.7 | 99.6 |
| $SiO_2$ | 21.6 | – | 0.25 | – |
| $Al_2O_3$ | 4.60 | – | – | 0.12 |
| $FeO_3$ | 0.33 | – | 0.02 | 0.03 |
| CaO | 67.5 | – | – | – |
| MgO | 0.59 | ≤10.0 | – | – |
| $SO_3$ | 2.83 | ≤4.0 | – | – |
| $Na_2O$ | 0.13 | – | – | – |
| $K_2O$ | 0.61 | – | – | – |
| Alkaline equivalent (in $Na_2O$) | 0.53 | – | – | – |
| CaO | 2.26 | – | – | – |
| Insoluble Residue – RI | 0.43 | ≤7.0 | – | – |
| $CO_2$ | 0.67 | ≤25.0 | – | – |

Note – Alkaline equivalent (in $Na_2O$) = $\%Na_2O + 0.658 \times \%K_2O$/LOI: Loss on ignition.

**Table 4**
Consumption, in kg/m$^3$, of each raw material.

| Composition | Ref | Ref+P25 | Ref+PC105 |
|---|---|---|---|
| WPC 40 | 115.1 | 114.1 | 114.1 |
| Dolomite # 20 | 67.3 | 66.7 | 66.7 |
| Dolomite # 40 | 378.4 | 375.1 | 375.1 |
| Dolomite # 80 | 104.1 | 103.2 | 103.2 |
| Water retainer | 1.5 | 1.5 | 1.5 |
| Air-entrainment | 0.2 | 0.2 | 0.2 |
| Deionized water | 332.0 | 365.2 | 349.1 |
| Polypropylene microfibers | 1.5 | 1.5 | 1.5 |
| n-$TiO_2$ (P25) | – | 4.5 | – |
| n-$TiO_2$ (PC105) | – | – | 4.8 |

through the contact area. The specimens were placed on grids, inside of a box containing a water height of 1 cm (Fig. 10). The water absorption of the specimens was determined by weighing in the following intervals: 0 h (dry mass), 15′, 30′, 1 h, 2 h, 4 h, 8 h, 24 h, and 48 h.

Dimensional variation (shrinkage): measured according to Brazilian standards, using 25 × 25 × 285 mm test specimens. The dimensional variation of the specimens was determined by a comparator clock with a resolution of 0.001 mm at intervals of 2 times a day, for 28 days, as shown in Fig. 11.

## 3. Results and discussion

### 3.1. Fresh state properties

Table 6 shows the spreading of mortars obtained by the flow-table test and the air-incorporation results. The rendering mortars must present spreading capacity to be considered adequate to be applied in facades. In the flow-table test, the spreading is considered a preponderant factor.

The Brazilian standard do not indicate an ideal flow result in flow-table tests. Based in previously conducted studies, the target for this kind of test was 220 ± 10 mm. In fact, the compositions that do not reach this range were rejected (Ref+P25p and Ref+PC105p with water constant).

The results indicate that it was not possible to maintain the same amount of kneading water as used in the reference mortars, because the addition of n-$TiO_2$ in the mixture required a higher water content. When the same water content used to prepare the reference mortars is maintained, there is a spreading detriment in all the mixtures.

With different specific surface areas, the different n-$TiO_2$ samples required different volumes of water for the same degree of spreading. Thus, for the amount of water added per n-$TiO_2$ samples, the mortar that presented the best spreading (workability) and with a lower volume of air incorporated was

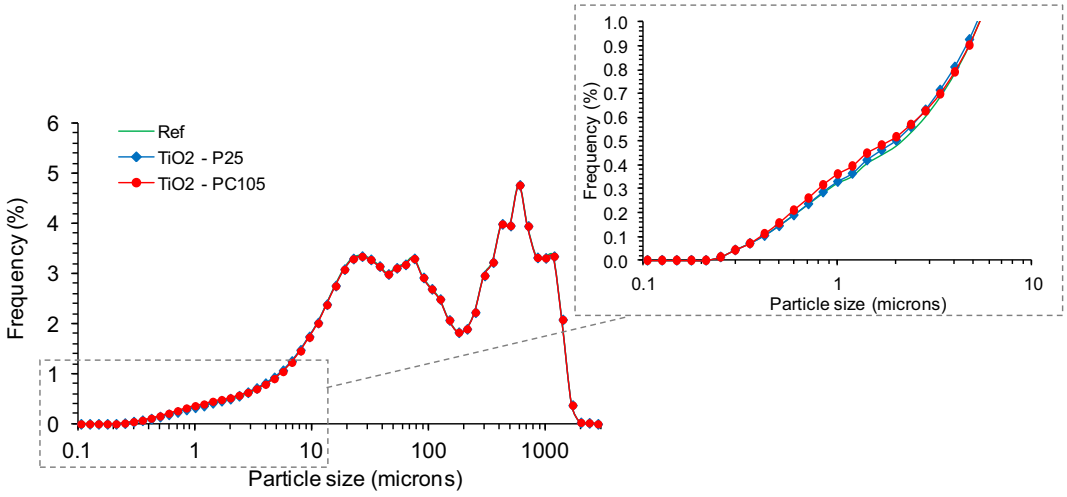


**Fig. 3.** Particle size distribution of each composition.

**Table 5**
Particle packing and mobility.

| Composition | Ref | Ref+P25 | Ref+PC105 |
|---|---|---|---|
| Packing porosity (%) | 8.7 | 8.5 | 8.5 |
| Packing porosity – finer particles (%) | 14.1 | 13.9 | 13.8 |
| Volumetric Surface Area ($m^2/cm^3$) | 1.79 | 3.08 | 3.88 |
| IPS (microns)* | 0.49 | 0.31 | 0.23 |
| MPT (microns)** | 16.9 | 18.0 | 17.6 |

* Interparticle separation.
** Maximum paste thickness.

the mortar Ref+P25d. This means that when the consistency of the mortars with the addition of n-$TiO_2$ is evaluated through the flow-table test and the volumes of water, the addition method and the n-$TiO_2$ sample used directly influence the results. Thus, the following steps of this study were carried out using only accepted compositions.

In the civil engineering sector, the squeeze flow method has been used to evaluate the rheological behaviour of pastes, plasters, extruded building materials and different types of mortars as an alternative complementary method. That method has been applied to simulate processing and application conditions such as difficulties in rotational techniques as slipping, material-shear element interfaces, measuring fiber-containing pastes. The test geometry changes during gap reduction and creates flow conditions similar to those that involve the processing and application of mortars, as pumping and spraying, spreading and finishing, squeezing between bricks.

The test consists in compressing a cylindrical specimen between two parallel polished metallic plates, as a reference condition, and controlling the displacement rate. Compared to other types of rheological method, this test does not simulate the most common problem that is the loss of contact between the material and the sheer element, especially for materials with plastic characteristics such as mortars. The method is adequate to evaluate both mixtures of any level of consistency and mixtures with the addition of fibers. In the case of rendering mortars, the test simulates the processing conditions as spreading, levelling and finishing. Fig. 12 shows the results obtained in the mortars 5 min after mixing, and Table 7 illustrates a quantitative evaluation.

In the flow table method, the mortars are evaluated as a function of their own weight. In the squeeze flow test simulates the mortars being applied to different spreading conditions and the better dispersion condition of the particles can result in lower compressive loads. In this study the results were considered for a 1 cm thick, and a 10 cm displacement mortar.

No differences were observed between the specimens with n-$TiO_2$-P25 and the reference, indicating that this type of titanium does not require high mixing energy for its dispersion. On the other hand, in the case of n-$TiO_2$-PC105 sample, there is a clear difference when comparing the squeeze flow spreading of the prepared samples with standard and high shear energy.

When the composition was mixed with (SEM), the presence of n-$TiO_2$-PC105 sample resulted in a higher load for the same compressive displacement, resulting from the higher agglomeration and retention of some of the water used to promote particle spacing and improve flow. On the other hand, with (HED) condition of n-$TiO_2$ promoted by the increase of the sheer energy, the spreading of this mortar was similar to that of the reference, showing that the agglomerates were broken, and the flow facilitated.

According to Romano et al [38], the use of (HED) is more efficient for the dispersion of fine particles compared to the (SEM). The authors applied the same concept used in this article and concluded that the use of (SEM) with lower shear energy did not result in a significant improvement in the dispersion, even with an increase in the mixing time, since the obtained particle size curves were similar and with coarser particles. On the other hand, the use of (HED) resulted in a reduction in coarser particles. Thus, it could be concluded that the higher dispersion efficiency is directly related to the increase in the population of particles with smaller diameters.

When it is observed the mortars Ref+P25 (powdered or dispersed) there is practically no difference in workability in the fresh state, as compared with the reference or between them. On the other hand, for the mortar Ref+PC105 in the dispersed form no difference was observed in comparison with the reference mortars, but when the (SEM) of n-$TiO_2$ was used (Ref+PC105p), the spreading showed a small changes, as it needed more effort to obtain the same displacement. In other words, the (HED) of n-$TiO_2$-PC105 resulted in an improvement in the workability of that mortar for conventional applications using spreading.

Comparing different samples of n-$TiO_2$, it is clear that using different dispersion condition of n-$TiO_2$ no-differences were observed between them, but the particle agglomeration in the (SEM) condition resulted in considerable differences. It is possible to observe that even after the application of (HED), n-$TiO_2$-PC105 presents a

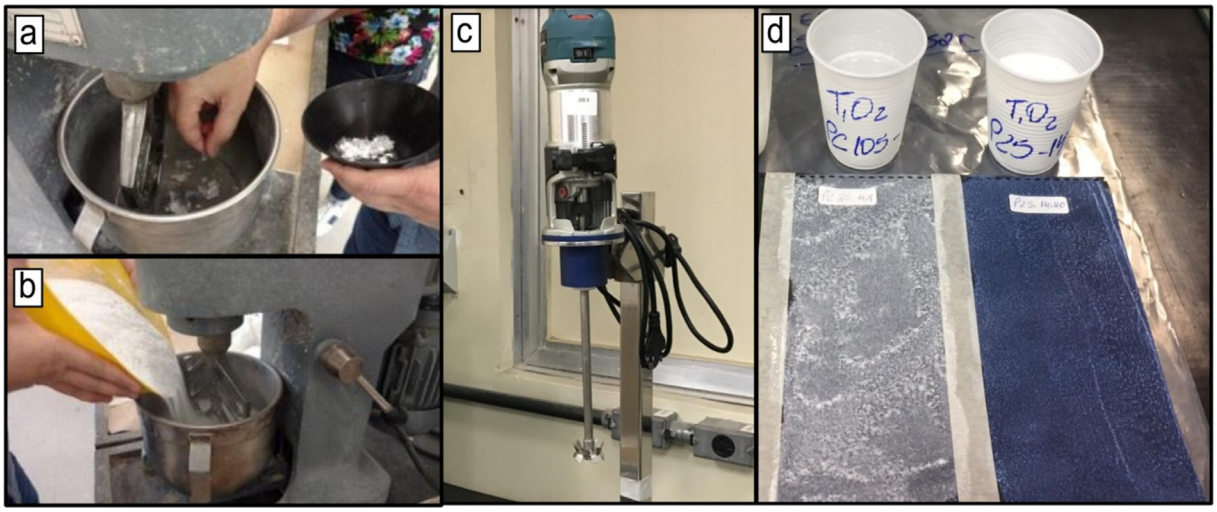


**Fig. 4.** SEM (a–b); HED equipment (c); suspension after HED (d).


**Fig. 5.** Consistency according to the flow table method.

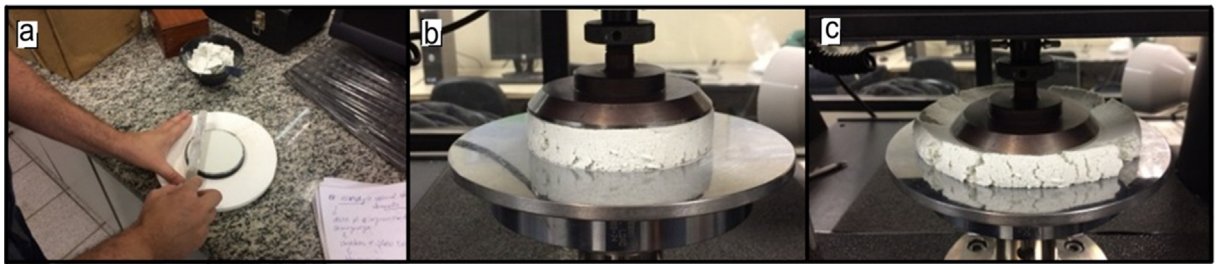


**Fig. 6.** Preparation of the sample (a); beginning (b) and; the end of the test (c).

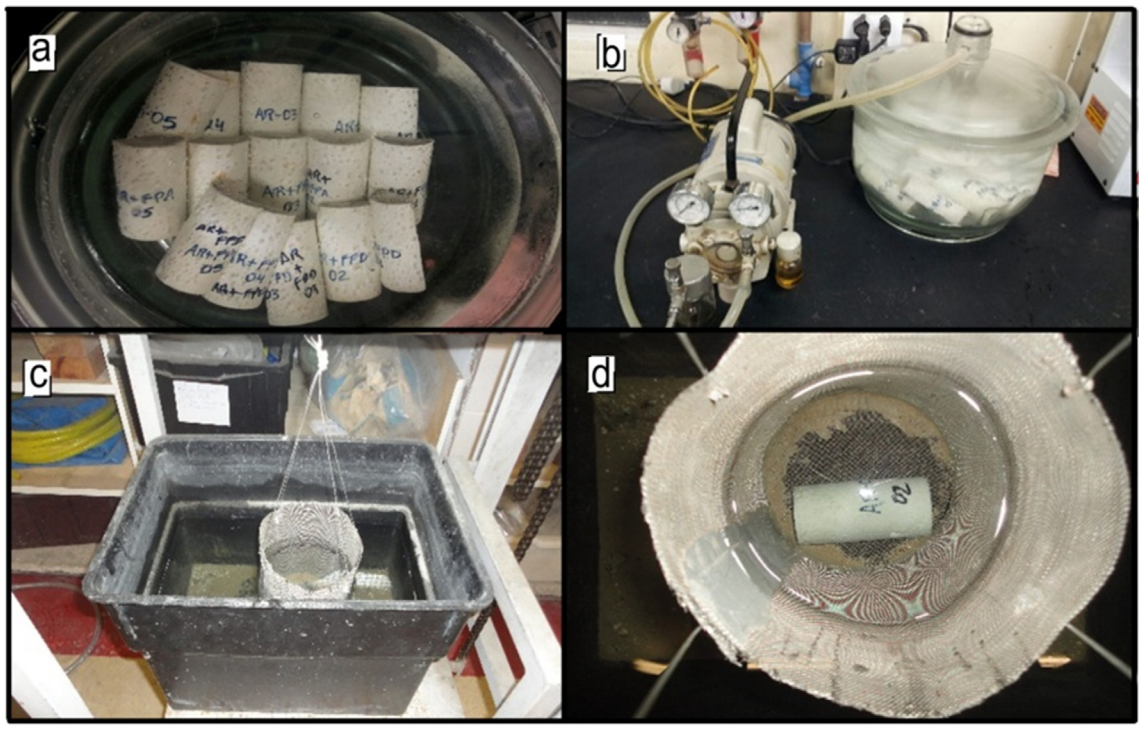


**Fig. 7.** Porosity test (Archimedes water immersion test). Note – Vacuum insertion (a–b); mass measurement (dry, wet, immersed – c–d).

higher concentration of clustered particles, showing a creamy consistency than n-$TiO_2$-P25 suspension, as shown in Fig. 4C, illustrating that n-$TiO_2$-PC105 would need more effort to be applied, and that can result in differences in the productivity and sometimes affecting the quality of the applied coating.

The results show that although the (HED) is an efficient method for the deagglomeration of n-$TiO_2$ particles, the impact of changing the mixing energy depended on the n-$TiO_2$ sample used.

### 3.2. Hardened state properties

The properties of n-$TiO_2$ were evaluated as a function of the dispersion condition. Fig. 13 summarizes the hardened properties results for each mortar, such as porosity, air-permeability, split tensile strength and modulus of elasticity, while the average results of the capillary coefficient for each mortar are shown in Fig. 14.

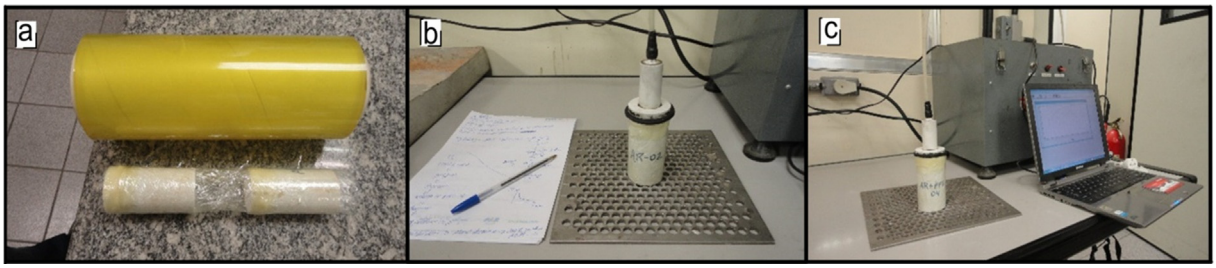


**Fig. 8.** Air-permeability. Note – Sample preparation (8a); Measurement process (b–c).

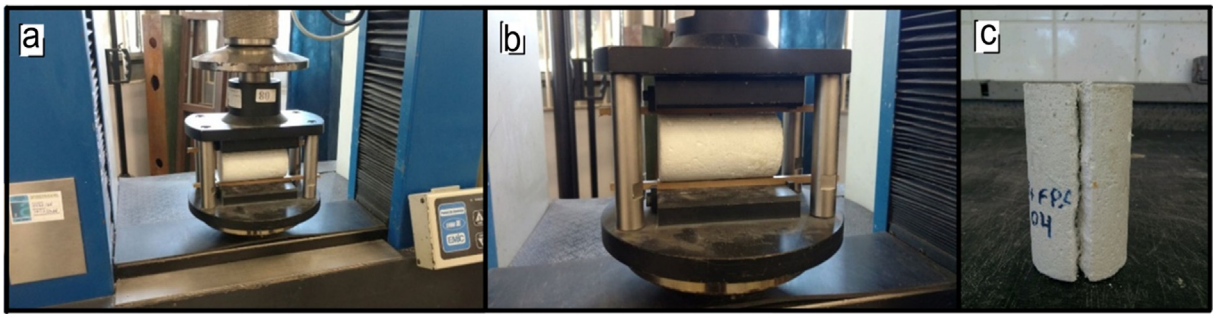


**Fig. 9.** Tensile strength in diametrical compression, according Brazilian standard. Note – Determination according Brazilian standard (a–b); specimen after test (c).


**Fig. 10.** Water absorption by capillarity. Note – Sample preparation (a); Sub-immersion process (b–c).

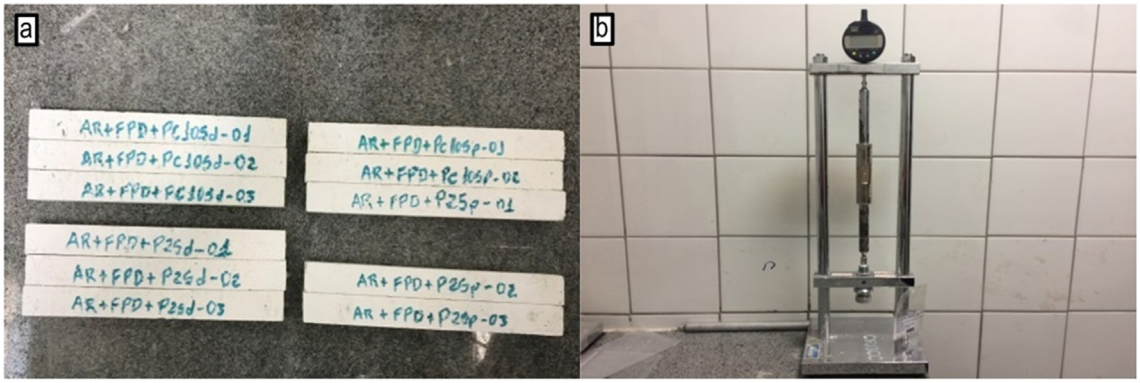


**Fig. 11.** Dimensional variation (Shrinkage). Note – Specimens (a); Comparator clock (b).

Mortar water content largely impacts mortar properties, it can have a stronger influence on mortar properties than binder type or the nature of the aggregate. Mortar porosity, density and water absorption are more significantly affected by water content than by aggregate quality [39]. Excessive water lowers a mortar's mechanical strength and increases the risk of fracturing by shrinkage.

The porosities of the mortars show differences when observed and comparing the samples and procedure of n-$TiO_2$ addition. For the addition of n-$TiO_2$ using the (HED) procedure, a lower porosity, regardless of sample, is observed when compared to the reference mortars. However, no significant differences were observed when comparing the two samples with each other, even with the granulometric differences between both. This is due to the addition

**Table 6**
Entrained air and flow table test results.

| Mixtures | Spreading (mm) | Entrained air (%) | Water added (g) |
|---|---|---|---|
| Reference Mortar | 227 ± 2.0 | 26.1 | 425.0 |
| Ref+P25p (water constant) | 178 ± 1.1 | – | 425.0 |
| Ref+P25p (consistency constant) | 219 ± 1.8 | 28.8 | 467.5 |
| Ref+P25d | 229 ± 3.7 | 24.3 | 467.5 |
| Ref+PC105p (water constant) | 203 ± 0.8 | – | 425.0 |
| Ref+PC105p (consistency constant) | 218 ± 0.5 | 27.0 | 447.0 |
| Ref+PC105d | 213 ± 2.0 | 25.5 | 447.0 |

procedure of the n-$TiO_2$ which did not allow a fast agglomeration of its particles during the mixing process and did not required a larger volume of water for the process of homogenization and workability of the mixtures. In relation to the (SEM), a better performance can be observed for sample n-$TiO_2$-PC105 in comparison with sample n-$TiO_2$-P25. As a very small particle, the direct addition procedure caused agglomeration of the n-$TiO_2$ particles during the mixing process, altering the workability and thus requesting a higher volume of water, as it can be observed in Table 6. This increase in water volume caused a direct impact on the porosity of the mortars, since allowing a larger amount of air caused a greater number of voids.

When comparing the split tensile strength versus the total porosity of the system in the experimental test, a moderate correlation ($R^2$ = 0.67) as expected. Was observed between a decrease in the split tensile strength and an increase in the porosity of the specimens. This is related to the fact that total porosity in the hardened state is a consequence of the air voids resulting from the air-entrainment and water content. As the aggregates normally used in the composition of these materials have a very low porosity and a mechanical resistance of 130 MPa or higher, the strength of conventional mortars is defined by the porosity of the hydrated cement paste added to the defects present in its microstructure [37,40]. For the five mixtures evaluated, the Ref+P25p mortar was the one that presented on average a lower tensile strength in the diametrical compression, since it has a greater total porosity, confirming the results previously found.

The total porosity and the dynamic modulus of elasticity of the mortars show a significant correlation ($R^2$ = 0.88). A decreasing trend line is observed, which means that a higher total porosity results in a smaller modulus of elasticity. The smaller the modulus, the higher is the deformation capacity of the mortar, thus reducing the possibility of cracking in the hardened state [41]. The reduction of the modulus of elasticity is paired with a reduction in the mechanical strength due to the increase in total porosity. Mechanical strength reduction may be a relevant factor in laying structural or even regular masonry, however, it does not seem to be of great importance for rendering mortars, except for adherence and integrity purposes. Following the same pattern of tensile strength, among the five mixtures evaluated, the mortar Ref+P25p presented the lowest values in the modulus of elasticity. In fact, the correlation between tensile strength and modulus of elasticity was very high in this study.

The evaluation of the dynamic modulus of elasticity versus air permeability also shows a good correlation ($R^2$ = 0.70). A downward trend is also observed, which means that a higher modulus of elasticity results in a lower air permeability because both properties are related to the porosity.

The greater the modulus, the lower the deformation capacity of the mortar, increasing the possibility of cracking in the hardened state, which is rather inappropriate for coating mortars. The increase in modulus of elasticity is paired with an increased tensile strength due to lower total porosity. However, no such relationships are observed for mortar Ref+P25d. Note that even with a lower total porosity, the mortar has a lower tensile strength, a lower modulus of dynamic elasticity and a higher air permeability when compared to mortar Ref+PC105d. That behaviour can be allied to the characteristics of n-$TiO_2$-P25 sample, where a greater

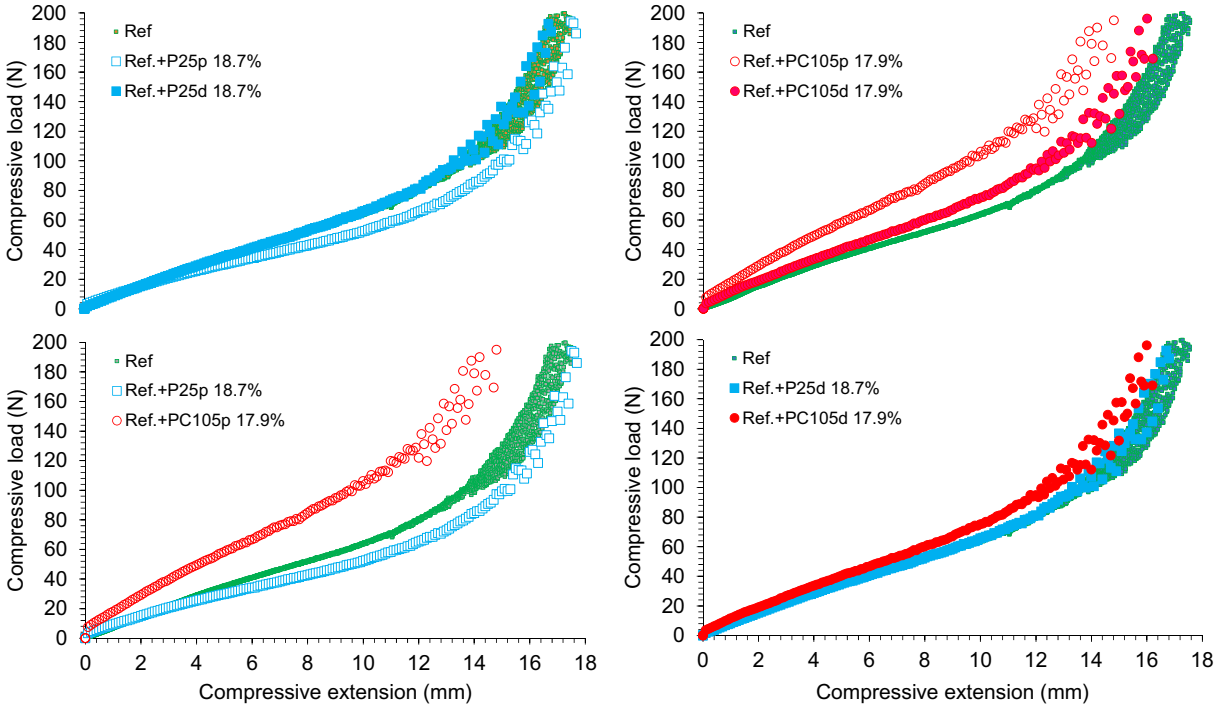


**Fig. 12.** Squeeze flow results. Percentage presented indicates the water content in each composition.

**Table 7**
Summary of load and displacement of the mortars in fresh state.

| Mixtures | Spreading Flow table (mm) | Load with displacement of 10 mm (N) | Displacement with 100N (mm) |
|---|---|---|---|
| Reference Mortar | 227 | 63.9 | 14.0 |
| Ref+P25p | 219 | 52.2 | 15.3 |
| Ref+P25d | 229 | 65.7 | 13.3 |
| Ref+PC105p | 218 | 106.2 | 9.6 |
| Ref+PC105d | 213 | 75.1 | 12.5 |

incorporation of air in the standard energy mix product and a higher amount of water used in the composition resulted in such porosity values and, thus, the changes in the hardened state that directly affected the modulus of elasticity.

Thus, considering the evaluated property and the results obtained, among the five mixtures evaluated, the reference mortar was the one with the lowest air permeability values, followed by the Ref+PC105d mortar due to its lower total porosity.

The mortar permeability at 28-days was evaluated by the capillary coefficient obtained by water absorption as a function of time. For water absorption tests on rendering mortars, all mixtures reached saturation after 48 h of sub-immersion. The addition of air-entraining additives in the mortars studied shows a larger internal air volume for the mortars containing powdered n-$TiO_2$, as shown in Table 6.

As far as the capillary coefficients obtained, the results showed that for the mixtures containing n-$TiO_2$ -P25 sample directly added or dispersed there was no difference between the two as regards water absorption, showing the same capillary coefficient, however, they showed a higher absorption index when compared to the others. For mixtures with the presence of n-$TiO_2$-PC105 sample, a lower absorption rate is observed when the compound is added to the mixture with high energy of dispersion (HED) procedure.

To determine the influence of n-$TiO_2$ dispersion in terms of statistical significance, two statistical methods were used: One-way ANOVA and the Tukey test. Those methods were used to indicate which dispersion method showed the lowest variation, as it can be observed, as an example, in Table 8, for tensile strength.

All parameters were evaluated statistically and performed in the same procedure. However, since the table would be the same in all cases, authors selected only one example of the data output in the Anova table. Table 9 presents a comparative summary of the values of F, $F_{critic}$ and Proof Value (p-value) to all parameters evaluated.

Although the One-way ANOVA test can demonstrate the existence of differences in the evaluated samples, it cannot clearly identify these differences and where they are. So, the Tukey's test was applied to compare the mortars in pairs and identify the real differences.

A paired Tukey test analysis showed that the compositions formulated with n-$TiO_2$-P25 sample, regardless of the n-$TiO_2$ dispersion process, showed meaningful changes in relation to the other

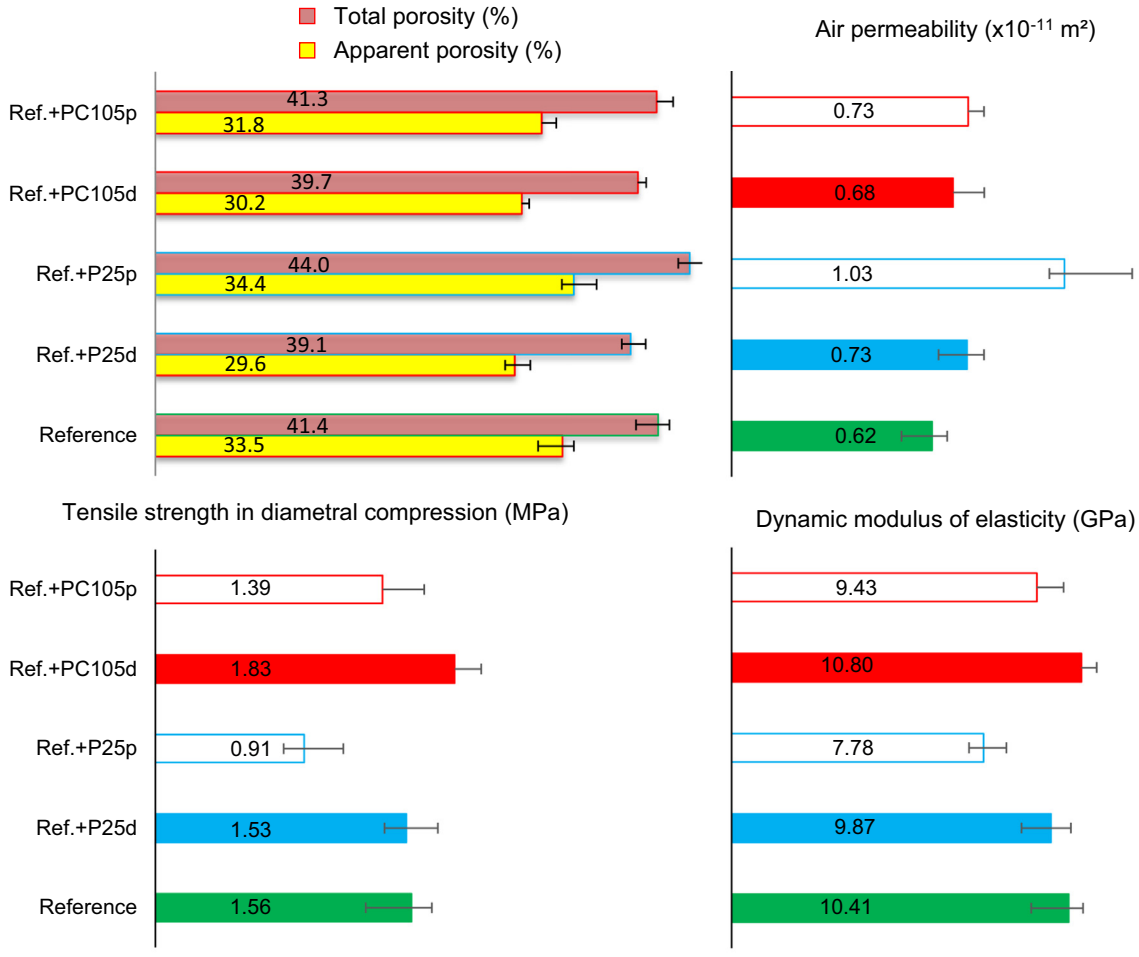


**Fig. 13.** Summary of hardened mortar properties.

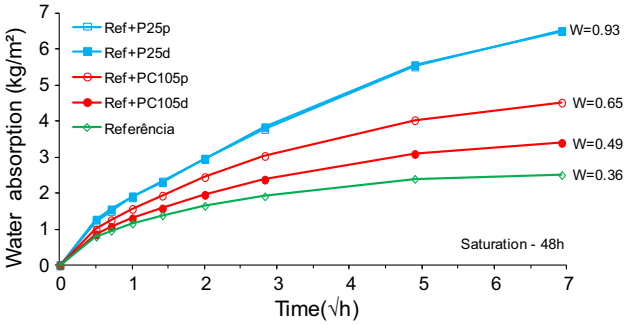


**Fig. 14.** Water absorption by capillarity (W, in kg/m$^2$ × $\sqrt{h}$). Note: Monitoring of Ref+P25 (d and p) were similar.

**Table 8**
Summary of statistical analysis of variance evaluating the impact of n-$TiO_2$ dispersion in the tensile strength.

| Group | Count | Sum | Average | Variance |
|---|---|---|---|---|
| AR-FPD | 5 | 7.82 | 1.56 | 0.02 |
| AR-FPD + P25d | 4 | 6.13 | 1.53 | 0.04 |
| AR-FPD + P25p | 5 | 4.55 | 0.91 | 0.06 |
| AR-FPD + PC105d | 5 | 9.13 | 1.83 | 0.03 |
| AR-FPD + PC105p | 5 | 6.94 | 1.39 | 0.06 |

| Source of variation | SQ | GL | MQ | Fcalc | P-value | F crític |
|---|---|---|---|---|---|---|
| Between groups | 2.28 | 4 | 0.570 | 14.10 | 1.7E-05 | 2.90 |
| In the groups | 0.77 | 19 | 0.040 | | | |
| Total | 3.05 | 23 | | | | |

compositions for all evaluated properties. In addition, when compared to each other, they also presented statistically significant differences, except for water absorption by capillarity, where the dispersion model showed no difference, as shown in Fig. 14.

The mortars with n-$TiO_2$-PC105 sample when compared to each other, as a function of the dispersion process presented differences only in relation to the results of the modulus of elasticity and tensile strength. When compared to n-$TiO_2$-P25 sample, they presented suggestive differences from the other compositions for all properties, demonstrating that those differences are from the characteristics of each n-$TiO_2$ and not directly from the dispersion procedure.

Comparisons with the reference mortars showed that for n-$TiO_2$-P25 sample, regardless of the dispersion procedure, there were statistical changes in the evaluated properties, except for air permeability and total porosity when used in powder. For n-$TiO_2$-PC105 sample, there were no statistically significant differences in the evaluated properties, except for capillary water absorption.

In sum, it has been observed that regardless of the n-$TiO_2$ samples, when the compound was more efficiently dispersed, the properties in the hardened state were more satisfactory, even though the amount of kneading water was maintained for each product. In other words, the dispersion process improved microstructural homogeneity and potentialized the effects of both cement and n-$TiO_2$ on the mixtures evaluated.

Figs. 15 and 16 show the evolution of the drying shrinkage as a function of time and the water amount for the five specimens. Each point in the graph corresponds to the average of the shrinkage values of three moulded samples to each specimen and the interval is also shown. Differences between specimens may occur as part of the error associated with the experimental process.

The results show the same trend in the drying shrinkage intensity at the beginning of the process. However, such results also show that the reference mortars exhibits a lower retraction when compared with others, this is due to the amount of kneading water used in the mixing.

It was observed that among the evaluated mortars containing n-$TiO_2$, those with the addition of the n-$TiO_2$-PC105 sample, were the ones that presented better performances in terms of shrinkage results. On the other hand, the drying shrinkage rate is much higher after 28-day period for mixtures with n-$TiO_2$-P25 sample, regardless of the dispersion procedure.

Results showed that when the compositions with different samples of n-$TiO_2$ are compared to each other, the dispersion

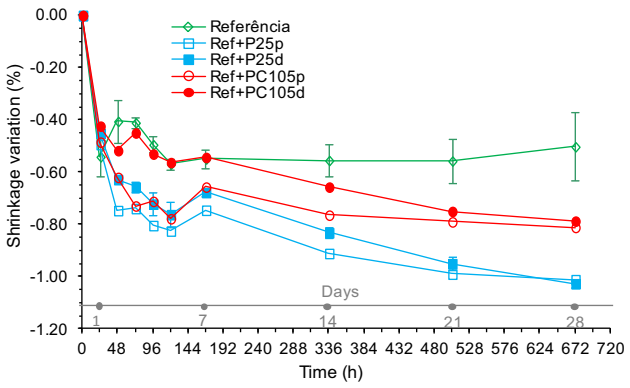


**Fig. 15.** Shrinkage variation over time.

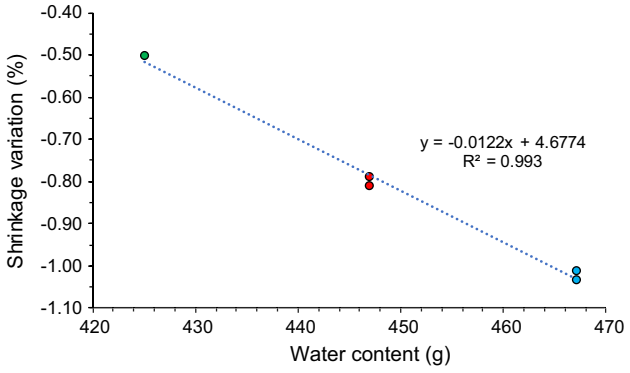


**Fig. 16.** Shrinkage variation by added water.

**Table 9**
Summary of statistical analysis of variance evaluating the impact of $TiO_2$ dispersion in others.

| Property | p-value | F | F-critic | Result |
|---|---|---|---|---|
| Total Porosity | 5.2E-05 | 11.49 | 2.87 | Statistically different |
| Apparent porosity | 4.7E-05 | 11.68 | 2.87 | Statistically different |
| Modulus of elasticity | 2.7E-06 | 17.43 | 2.87 | Statistically different |
| Tensile strength | 1.7E-05 | 14.10 | 2.90 | Statistically different |
| Air-permeability | 5.6E-04 | 8.56 | 2.96 | Statistically different |
| Water absorption by capillarity – W | 4.6E-08 | 28.95 | 2.87 | Statistically different |

procedure makes no difference in shrinkage after 28-day period, but rather the sample of n-$TiO_2$ and amount of water used in the mixtures.

## 4. Conclusions

Based on the results obtained, the main considerations of this study are:

- although the parameters of mobility and particle packing were used to define the mortars compositions, no correlation was observed in the resulting properties.
- the dispersion condition showed a significant change in spreading in all the mortars. When the consistency of the mortars with n-$TiO_2$ addition was evaluated by means of the flow-table test using the same volumes of water, the addition method and the n-$TiO_2$ sample used directly influenced the results. It means that when n-$TiO_2$ is dispersed in a Standard Energy Mix (SEM), there is a difference in spreading. When n-$TiO_2$ is dispersed in a high energy (HED), no difference was observed in squeeze flow spreading.
- in the hardened state, porosity, tensile strength, modulus of elasticity, air-permeability and water absorption by capillarity were statistically different from the properties observed for the reference composition and in a function of the dispersion methods and the n-$TiO_2$ sample evaluated.
- it was observed that, regardless the n-$TiO_2$ sample, when the compound was more efficiently dispersed, the properties in the hardened state were more satisfactory, even though the amount of kneading water was maintained for each product. In other words, the dispersion process improved microstructural homogeneity, potentializing the effects of the cement and n-$TiO_2$ on the mixtures.
- in terms of drying shrinkage results, that phenomenon is associated to the n-$TiO_2$ sample and the amount of water used in the mixture and not with the n-$TiO_2$ dispersion procedure. The effect of the n-$TiO_2$ on dimensional variation control is potentially increased by dispersion since it guarantees n-$TiO_2$ homogeneity on rendering mortars.

## Conflict of interest

None.

## Acknowledgements

The authors wish to thank the Laboratory of Microstructure and Material Eco-efficiency – LME and the Institute of Technological Research (IPT) and its foundation (FIPT) for financial and institutional support to carry out the experimental stage, through the New Talents Program N°01/2017. The Coordenação de Aperfeiçoamento de Pessoal de Nível Superior – Brazil (CAPES) – Finance Code 001, and the Research Foundation of the State of São Paulo (FAPESP) [Grant N°2016/14473-6 (Kai Loh)] for their financial support, and Cristal Pigmentos do Brasil, Votorantim cimentos SA, Neo-Matex (fibras e têxteis técnicos para engenharia) and the Ibratin Industria e Comércio Ltda for their material support to this research work.

## Appendix A. Supplementary data

Supplementary data to this article can be found online at https://doi.org/10.1016/j.conbuildmat.2019.04.190.

## References

[1] P. Mikuláček, R.J. Wakeman, J.Q. Marchant, The influence of pH and temperature on the rheology and stability of aqueous titanium dioxide dispersions, Chem. Eng. 67 (1997) 97–102.
[2] L. Senff, J.A. Labrincha, V.M. Ferreira, D. Hotza, W.L. Repette, Effect of nano-silica on rheology and fresh properties of cement pastes and mortars, Constr. Build. Mater. 23 (2009) 2487–2491.
[3] L. Senff, D. Hotza, W.L. Repette, V.M. Ferreira, J.A. Labrincha, Effect of nanosilica and microsilica on the microstructure and the hardened properties of cement pastes and mortars, Adv. Appl. Ceram. 109 (2010) 104–110.
[4] I.R. Oliveira et al., Particle Dispersion and Packaging, Fazendo Arte, São Paulo, 2000 [in Portuguese].
[5] J. Plank, C. Hirsch, Impact of zeta potential on early cement hydration phases on superplasticizer adsorption, Cem. Concr. Res. 37 (2007) 537–542.
[6] B.L. Damineli, Concepts for Formulation of Concretes with Low Consumption of Ligants: Rheological Control, Packaging, and Dispersion of Particles 2013. 265 f. Thesis (PhD) – Civil Engineering Course, Civil and Urban Construction Engineering, Polytechnic School of the University of São Paulo, São Paulo, 2013 [in Portuguese].
[7] J.V.S. Melo, G. Trichês, Study of the influence of nano-$TiO_2$ on the properties of Portland cement concrete for application on road surfaces, Road Mater. Pavement Des. 19 (2017) 1011–1026.
[8] L. Pinho, M.J. Mosquera, Photocatalytic activity of $TiO_2$–$SiO_2$ nanocomposites applied to buildings: influence of particle size and loading, Appl. Catal. B 134–135 (2013) 205–221.
[9] M.H. Maciel, H.M. Bernardo, G.S. Soares, R.C. de O. Romano, M.A. Cincotto, R.G. Pileggi, Effect of the variation of cement consumption on coating mortars produced based on the concepts of mobility and packaging of particles, Ambiente Construido 18 (2018) 245–259 [in Portuguese].
[10] F. Sanchez, K. Sobolev, Nanotechnology in concrete – a review, Constr. Build. Mater. 24 (2010) 2060–2071.
[11] M. Lackhoff et al., Photocatalytic activity of semiconductor-modified cement: influence of semiconductor type and cement ageing, Appl. Catal. B 43 (2002) 205–2016.
[12] ASTM C1365-06: Standard Test Method for Determination of the Proportion of Phases in Portland cement and Portland-Cement Clinker Using X-ray Powder Diffraction Analysis, 2011.
[13] ABNT, NBR NM 18: Portland cement – Chemical analysis – Determination of fire loss, item 5.1, Rio de Janeiro, 2012 [in Portuguese].
[14] ABNT, NBR NM 11-2: Portland cement – Chemical analysis - Optional method for determination of major oxides by complexometry – Part 2: Method ABNT, items 5.1.2 a 5.2.4, Rio de Janeiro, 2012 [in Portuguese].
[15] ABNT, NBR NM 16: Portland cement – Chemical analysis – Elective method – Determination of sulphuric anhydride, Rio de Janeiro, 2012 [in Portuguese].
[16] ASTM C114-15: Standard Test Methods for Chemical Analysis of Hydraulic Cement.
[17] ABNT, NBR 13810: Determination of metals – Atomic Absorption Spectrometry Method, Rio de Janeiro, 1997 [in Portuguese].
[18] ABNT, NBR NM 13: Portland Cement – Chemical Analysis – Determination and Free Calcium Oxide by Ethylene Glycol, Rio de Janeiro, 2013 [in Portuguese].
[19] ABNT, NBR NM 22: Portland cement with additions of pozzolanic materials – Chemical analysis – Arbitrage method, item 6.7, Rio de Janeiro, 2012 [in Portuguese].
[20] ABNT, NBR NM 20: Portland cement and its raw materials – Chemical analysis – Determination of carbon dioxide by gasometry, Annex B, Rio de Janeiro, 2012 [in Portuguese].
[21] R.C.O. Romano, F.A. Cardoso, R.G. Pileggi, Concrete properties in the fresh state. In: ISAIA, G. C. Concrete: Science and Technology. São Paulo: Arte Interativa, 2011 [in Portuguese].
[22] H.J.H. Brouwers, H.J. Radix, Self-compacting concrete: theoretical and experimental study, Cem. Concr. Res. 35 (2005) 2116–2136.
[23] I. Marquardt, Determination of the composition of self-compacting concretes on the basis of the water requirements of the constituent materials – presentation of a new concept, Betonwerk + Fertigteiltechnik – BFT 11 (2002) 22–30.
[24] R.C.O. Romano, D.R. Torres, R.G. Pileggi, Impact of aggregate grading and air-entrainment on the properties of fresh and hardened mortars, Constr. Build. Mater. 82 (2015) 219–226.
[25] F.A. Cardoso, V.M. John, R.G. Pileggi, Rheological behavior of mortars under different squeezing rates, Cem. Concr. Res. 39 (2009) 748–753.
[26] ABNT, NBR 13276: Mortar for laying and coating of walls and ceilings – Determination of consistency index, Rio de Janeiro, 2016 [in Portuguese].
[27] ABNT, NBR 15839: Laying mortar and coating of walls and ceilings – Rheological characterization by the squeeze-flow method, Rio de Janeiro, 2010 [in Portuguese].
[28] ABNT, NBR 13278: Mortar for laying and coating of walls and ceilings – Determination of mass density and built-in air entrained, Rio de Janeiro 2005 [in Portuguese].
[29] ABNT, NBR 15259: Mortar for laying and coating walls and ceilings – Determination of water absorption by capillarity and capillary coefficient, Rio de Janeiro, 2005 [in Portuguese].
[30] ABNT, NBR 15630: Mortar for laying and coating of walls and ceilings – Determination of dynamic modulus of elasticity through ultrasonic wave propagation, Rio de Janeiro, 2009 [in Portuguese].

[31] ABNT, NBR 7222: Concrete and mortar – Determination of tensile strength by diametrical compression of cylindrical specimens, Rio de Janeiro 2011 [in Portuguese].
[32] ABNT, NBR 15261: Mortar for laying and coating of walls and ceilings – Determination of dimensional variation (shrinkage or linear expansion), Rio de Janeiro, 2005 [in Portuguese].
[33] SALVADOR G.A.B. Optimization of aggregates granulometric distribution for use in rendering mortar in Santana do Livramento – RS. Thesis (MSc); 2005 [in Portuguese].
[34] S.M.S. Selmo, Finer aggregates to rendering mortars, in: Simpósio Nacional de Materiais de Construção: Agregados, São Paulo, 1986, pp. 27–43 [in Portugese].
[35] R.C.O. Romano, Air incorporation in cementitious materials applied in civil construction. Thesis (PhD), Polytechnic School of the University of São Paulo. Department of Civil Construction Engineering, 2013, p. 200 [in Portuguese].
[36] M.D.M. Innocentini, V.P. Rodrigues, R.C.O. Romano, R.G. Pileggi, G.M.C. Silva, J. R. COURY, Permeability optimization and performance evaluation of hot aerosol filters made using foam incorporated alumina suspension, Hazard. Mater. 162 (2009) 212–221.
[37] V.A. Quarcioni et al., Estimation of porosity of cement and lime mortars by volume calculation method, Ambiente Construido 4 (2009) 175–187 [in Portuguese].
[38] R.C.O. Romano et al., Influence of the dispersion process in the silica fume properties, Ceramica. 54 (2008) 456–461 [in Portuguese].
[39] S. Pavía, B. Toomey, Influence of the aggregate quality on the physical properties of natural feebly-hydraulic lime mortars, Mater. Struct. 41 (2008) 559–569.
[40] P.K. Mehta, P.J.M. Monteiro, Concrete: microstructure, properties and materials. São Paulo: Ibracon, (2008) P. 674. [in Portuguese].
[41] Silva, N. G. da et al. Effects of air incorporated in the properties of the hardened state in mortars with cement and sand. IN: Congress Brasileiro Concrete, 51, 2009, Curitiba. Anais. Curitiba: Ibracon, 2009 [in Portuguese].